Variation of structural parameters in dimethylammonium manganese formate $[(CH_3)_2NH_2]Mn(HCOO)_3$ by substitution of transition metals (M = Zn, Co and Ni): by powder XRD method

D. Sornadurai,[1,a] R. M. Sarguna,[1] and V. Sridharan[1,2]
[1]*Condensed Matter Physics Division, Materials Science Group, Indira Gandhi Centre for Atomic Research, Kalpakkam, Tamil Nadu, India*
[2]*HBNI, Kalpakkam, Tamil Nadu, India*

(Received 18 October 2018; accepted 13 March 2019)

Variation of structural parameters of dimethylammonium manganese formate $[(CH_3)_2NH_2]Mn[(HCOO)_3]$ upon substitution by the transition elements Zn, Co, and Ni is studied by powder X-ray diffraction (PXRD) technique. These metal–organic framework (MOF) crystals were grown by solvothermal method. The PXRD patterns of all MOFs exhibited rhombohedral structure. PXRD patterns of MOFs were analyzed using Rietveld refinement method. While the parent Mn-MOF and $Mn_{0.9}Zn_{0.1}$MOF are found to have similar structural parameters, Co and Ni substituted Mn-MOFs have smaller structural parameters than that of parent Mn-MOF. The reason for this variation in the lattice parameters is explained based on the Shannon ionic radii. © *2019 International Centre for Diffraction Data*. [doi:10.1017/S0885715619000307]

Key words: Metal Organic Frameworks, Crystal Structure, Laue diffraction, Powder XRD method, Rietveld refinement, Shannon ionic radius

I. INTRODUCTION

Perovskite-type metal–organic framework (MOFs) materials have a general formula ABX_3. B-cations can either be divalent or trivalent transition metals like $B^{2+} = Mn^{2+}$, Fe^{2+}, Co^{2+}, and Ni^{2+} and $B^{3+} = Cr^{3+}$ and Fe^{3+}. B-cations occupy the center of the BO_6 octahedron. These octahedra are connected by X-anions known as linkers forming a three-dimensional scaffold arrangement. The voids at the center of these scaffolds are filled with A-cations, resulting in Perovskite-type MOFs (shown in Figure 1). There exists a broad choice for A-cations and X-anions. This offers a wide scope to tune its structure and thereby to modify the physical properties. Amongst the possibilities, most popular choice of linker X-anion and A-cation is the formate $(HCOO)^-$ and dimethylammonium $(DMA)^+$, respectively.

They have recently attracted the attention of researchers amongst others because of their multiferroic property (Jain *et. al.*, 2009). Upon cooling, these MOFs undergo a structural transition from non-polar $R\bar{3}c$ to polar Cc (Sánchez-Andújar *et. al.*, 2010). This structural transition drives the system from a high-temperature disordered paraelectric to a low-temperature long-range ordered antiferroelectric in the temperature range 160–185 K, depending upon the transition metal B-cation. The ferroelectric property is ascribed to the hydrogen bonding between H^+ of $(DMA)^+$ ion and O^- of $(HCOO)^-$ ion (Wang *et. al.*, 2013). At lower temperatures, ~8–36 K, they also undergo paramagnetic to canted antiferromagnetic transition rendering them to be multiferroic (Baker *et. al.*, 2010). Such a vast temperature difference between these two phase transitions shows weak coupling between electric and magnetic properties (Thomson *et. al.*, 2012). To alleviate this, among other possibilities divalent substitution at Mn site of Mn-MOF is being fervently followed (Zhao *et. al.*, 2017). As the desired properties depend on the structural parameters, it is of great importance that they are estimated. With this in view, we have carried out 10 at.% substitution at Mn site of the MOF with Zn, Ni, and Co. Structural parameters were estimated using Rietveld analysis of powder X-ray diffraction (PXRD) pattern.

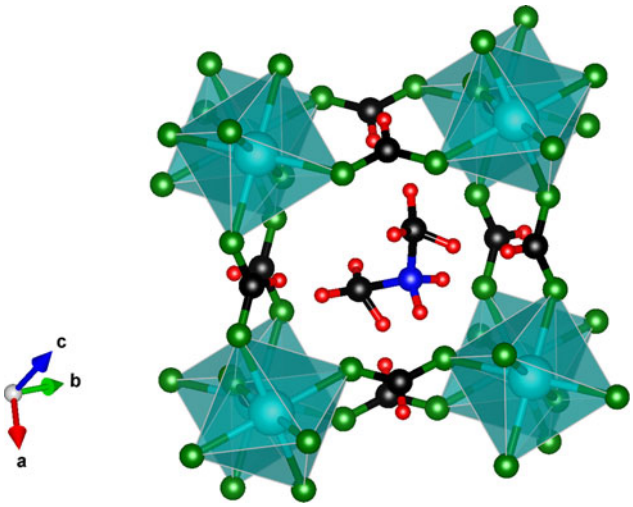

Figure 1. The Perovskite structure of Mn-MOF which is the basic building block of the Perovskite MOF.

[a]Author to whom correspondence should be addressed. Electronic mail: sorna@igcar.gov.in

TABLE I. Metallic ratios in the MOFs obtained from EDAX analysis.

Material	Composition of Mn and TM in at.%		Composition of Mn and TM in wt.%	
	Mn	TM	Mn	TM
Mn-MOF	100	0	100	0
Mn-Ni MOF	89.74	10.26	89.12	10.88
Mn-Co MOF	90.40	9.60	89.77	10.23
Mn-Zn MOF	89.38	10.62	87.61	12.39

II. EXPERIMENTAL

A. Crystal growth

Single crystals of $[(CH_3)_2NH_2]Mn(HCOO)_3$ as well as $[(CH_3)_2NH_2]Mn_{0.9}M_{0.1}(HCOO)_3$ (M = Zn, Ni, and Co) were grown by solvothermal reaction followed by slow evaporation quite similar to the growth of other MOFs (Mączka *et al.*, 2013). Commercially available precursor materials were used without further purification. In a typical crystal growth of Mn-MOF, 5 mM of $MnCl_2 \cdot 4H_2O$ was dissolved in 40 ml dimethylformamide and 40 ml deionized water stirred vigorously for a minimum of 30 min. In the case of 10 at.% Zn, Co, and Ni substituted Mn-MOFs, crystals were grown by mixing 4.5 mM $MnCl_2 \cdot 4H_2O$ with 0.5 mM of respective metal chlorides. The solution was transferred to a Teflon-lined stainless steel autoclave of 100 ml capacity and sealed well. The solvothermal reaction was carried out for 3 days at 140°C and was allowed to furnace cool. The supernatant solution was transferred to a beaker and left undisturbed for 7 days at room temperature for crystal growth. Grown crystals were harvested by filtering and washed using ethanol several times, dried at room temperature, and the dried crystals kept in a vacuum desiccator.

B. Composition analysis

The Mn-transition metal ion ratios of the crystals were analyzed using energy-dispersive X-ray analysis (EDAX) technique which is available in scanning electron microscopy (SEM) instrument (SEM-Carl Zeiss FE-SEM model, Supra 55; EDAX – Oxford instruments). The crushed crystals were spread on the carbon tape and placed on the SEM sample holder. When high-energy (~20 kV) electrons hit on the sample surface, characteristic X-ray of the elements emitted, which was recorded as EDAX spectra. From these spectra, the at.% and wt.% of Mn, Zn, Ni, and Co compositions were determined.

C. Laue diffraction

Laue diffraction on selected crystals were carried out using Mo target in the back-scattered geometry using an imaging plate. Because of smaller size, crystals were glued to a sharp tip of Kapton foil and mounted on to a goniometer. Care was taken that the collimated X-ray beam (0.5 mm) was incident perpendicular to the surface of the crystals. The exposed imaging plate was off-line scanned using an imaging plate reader. The Laue diffraction image was converted to digital imaging and communications in medicine (DICOM) format. The DICOM image file was processed using the freely available software ImageJ and stored in JPG format (Schneider *et al.*, 2012).

D. Powder X-ray diffraction

Room temperature PXRD measurements were carried out on well-crushed single crystals of respective MOFs. Diffraction patterns were recorded using a STOE X-ray diffractometer (STOE, Darmstadt, GmbH) operated in Bragg–

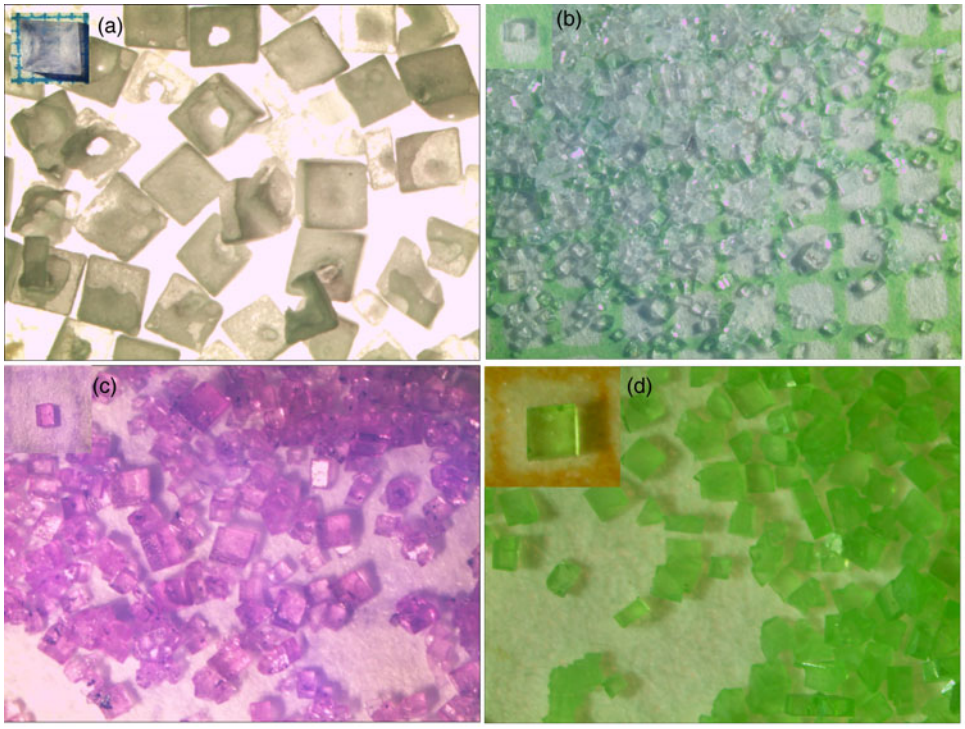

Figure 2. As grown crystals of (a) Mn-MOF, (b) $Mn_{0.9}Zn_{0.1}$-MOF, (c) $Mn_{0.9}Co_{0.1}$-MOF, and (d) $Mn_{0.9}Ni_{0.1}$-MOF crystals. The inset in "a" is in a 5 mm × 5 mm square size graph sheet, whereas in "b", "c", and "d" are in a 1 mm × 1 mm square graph sheet.

https://doi.org/10.1017/S0885715619000307 Published online by Cambridge University Press

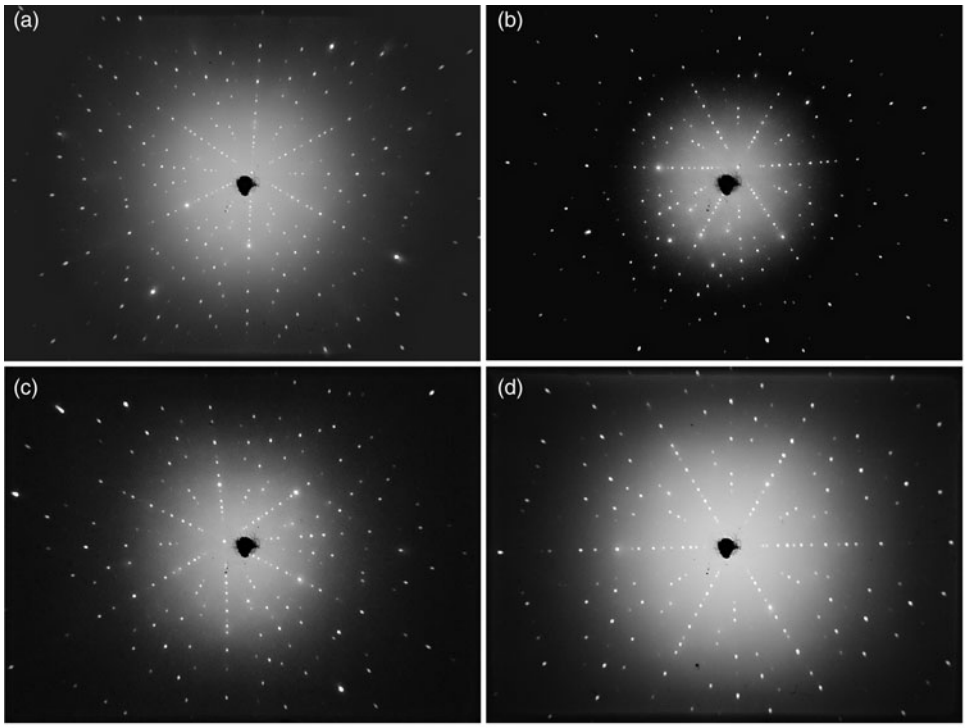

Figure 3. The back-scattered Laue diffraction pattern of as grown crystals of (a) Mn-MOF, (b) $Mn_{0.9}Zn_{0.1}$-MOF, (c) $Mn_{0.9}Co_{0.1}$-MOF, and (d) $Mn_{0.9}Ni_{0.1}$-MOF crystals.

Brentano geometry and in θ–θ mode. The diffraction patterns were recorded using Cu$K\alpha$ radiation and data were collected at a step size of 0.05° 2theta and with a counting time of 7 s step^{-1}. The diffracted X-ray was detected using a point detector attached along with a secondary monochromator. The detector made up of NaI:Tl scintillation crystal connected to a photomultiplier tube was used.

III. RESULTS AND DISCUSSIONS

A. EDAX results

The EDAX results showed the presence of C, O, N, Mn and the transition metals. But for calculating the Mn–transition metals ratios, the presence of C, O, N atoms is ignored and only Mn and substituted transition metals are considered. From this analysis, it was found that the ratio of Mn to transition metals has maintained nearly 0.96–0.11 closely matching with nominal composition. The obtained results are given in Table I. In the Rietveld refinement, occupancy factors were refined and it varied between 0.9 and 0.873 for Mn and the other transition elements varied from 0.1 to 0.127 in the refinement.

B. Optical micrograph

The optical micrographs of harvested MOF crystals are recorded by keeping them in a 1 mm graph paper [Figures 2(a)–2(d)]. The crystals exhibit well-defined facets with cubic and cuboidal morphologies. The size of Mn-MOF crystal is nearly 4 mm × 4 mm, whereas the sizes of the substituted crystals are of the order of 250–750 μm. Even though bigger size crystals are there in the substituted crystals, whatever brought inside the square of the graph sheet is captured and depicted. All the crystals are transparent though they differ in their

TABLE II. Crystallographic details of dimethylammonium manganese formate.

				Coordinates			
Sl. No	Atom	Wyckoff letter	Multiplicity	*x*	*y*	*z*	SOF
1	C	c	12	0.0000	0.0000	0.19712	1.0
2	H	f	36	−0.0211	0.1045	0.1864	0.333
3	H	f	36	−0.049	−0.0875	0.1604	0.333
4	H	f	36	0.1339	0.0468	0.1979	0.333
5	N	e	18	−0.0878	−0.0878	0.25	0.333
6	H	f	36	−0.2148	−0.1115	0.25	0.167
7	H	f	36	−0.1115	−0.2147	0.25	0.167
8	Mn	b	6	0.0000	0.0000	0.0000	1.0
9	O	f	36	−0.21069	−0.22087	0.05433	1.0
10	C	e	18	−0.3333	−0.2154	0.0833	1.0
11	H	e	18	−0.3333	−0.104	0.0833	1.0

https://doi.org/10.1017/S0885715619000307 Published online by Cambridge University Press

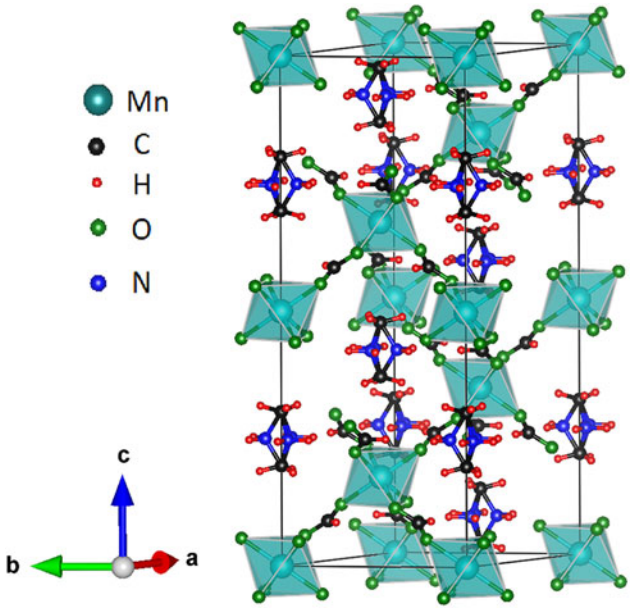

Figure 4. The rhombohedral crystal structure of dimethylammonium manganese formate with the general formula $[(CH_3)_2Mn](HCOO)_3$ in hexagonal coordinate system.

color. The intrinsic color is because of the crystal field splitting of the *d*-orbitals of transition metal ions occupying the octahedral site. While Mn- and 10 at.% Zn substituted MOF crystals are colorless, 10 at.% substituted Ni- and Co-MOFs exhibit green and pink colors, respectively.

C. Laue diffraction

The Laue diffraction patterns of the Mn-MOF, $Mn_{0.9}Zn_{0.1}$-MOF, $Mn_{0.9}Co_{0.1}$-MOF, and $Mn_{0.9}Ni_{0.1}$-MOF crystals were recorded [Figures 3(a)–3(d)]. The diffraction patterns exhibit sharp dots, indicating high crystalline nature of the crystals. Also, the Laue patterns have same symmetry indicating same crystal symmetry of the MOFs.

D Structural analysis

The powder XRD patterns of Mn-, $Mn_{0.9}Zn_{0.1}$-, $Mn_{0.9}Co_{0.1}$-, and $Mn_{0.9}Ni_{0.1}$-MOFs were recorded. Mn-MOF crystallizes in the rhombohedral structure with $R\bar{3}c$ space group (S.G. No. 167). The standard data of Mn-MOF from ICDD file No. 01-083-6748 were used as a model data for Rietveld refinement and tabulated in Table II (Figure 4). This pattern provides a reasonable fit to the measured data of Mn-MOF and hence used for the refinement of all the four

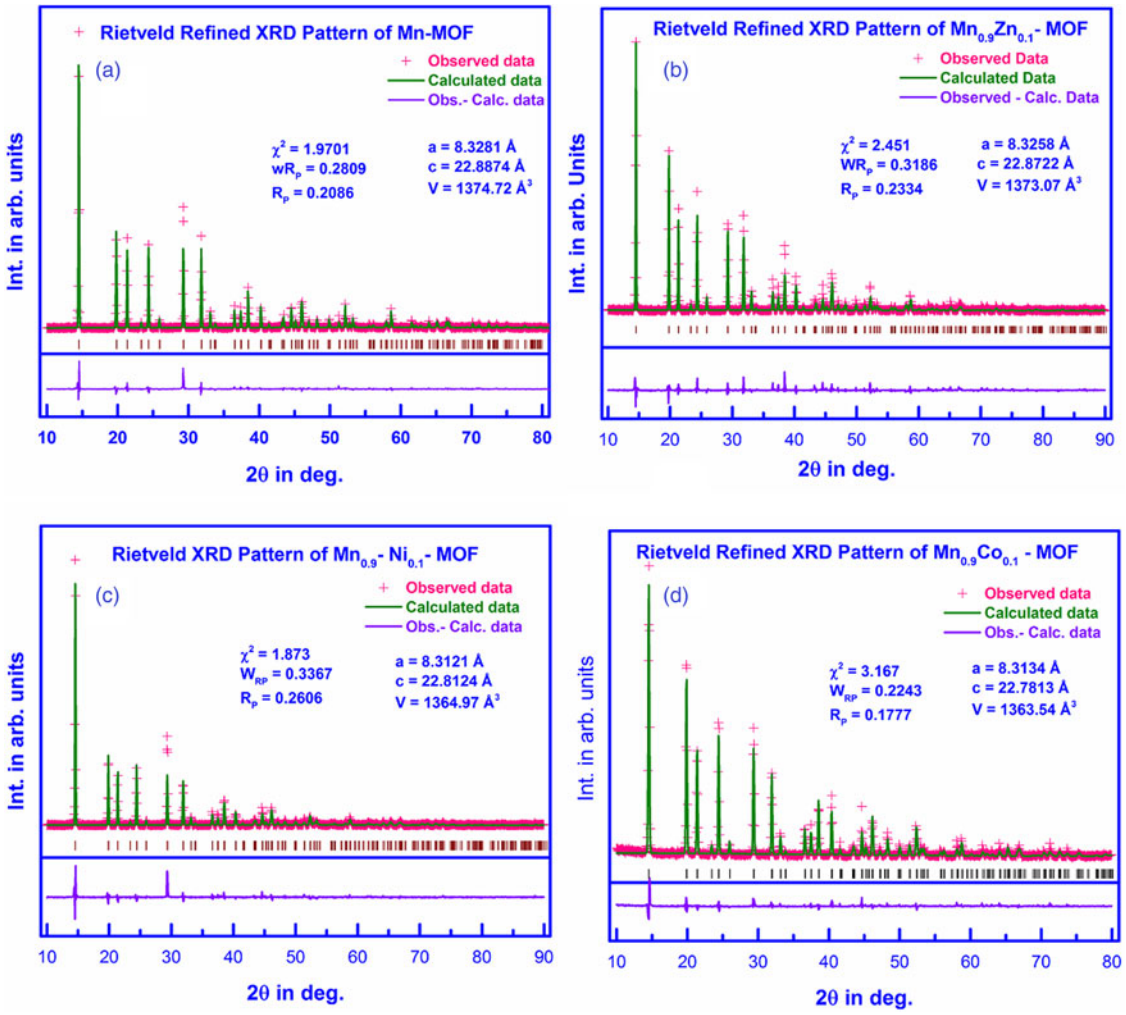

Figure 5. The Rietveld refined XRD patterns of powdered crystals of (a) Mn-MOF, (b) $Mn_{0.9}Zn_{0.1}$-MOF, (c) $Mn_{0.9}Co_{0.1}$-MOF, and (d) $Mn_{0.9}Ni_{0.1}$-MOF.

https://doi.org/10.1017/S0885715619000307 Published online by Cambridge University Press

TABLE III. Crystallographic parameters of $[(CH_3)_2NH_2]Mn_{0.9}M_{0.1}(HCOO)_3$ (M = Zn, Co, and Ni).

Material	a	c	V	W_{RP}	R_P	χ^2
Mn_MOF	8.3281 ± 0.00003	22.8874 ± 0.00016	1374.72 ± 0.011	0.2809	0.2087	1.970
$Mn_{0.9}Zn_{0.1}$	8.3258 ± 0.00001	22.8722 ± 0.00003	1373.07 ± 0.003	0.3186	0.2334	2.451
$Mn_{0.9}Ni_{0.1}$	8.3121 ± 0.00001	22.8124 ± 0.00005	1364.97 ± 0.004	0.3367	0.2606	1.873
$Mn_{0.9}Co_{0.1}$	8.3134 ± 0.00001	22.7813 ± 0.00005	1363.54 ± 0.004	0.2243	0.1777	3.6T7

data sets. Peak positions match well, but there is some difference in intensity ratio. No additional peaks could be discerned indicating phase purity of the sample. No change in the diffraction pattern of the substituted MOFs could be observed except for the shift in the Bragg reflections. This signifies the absence of structural transition upon 10 at.% substitution of Zn, Co, and Ni in Mn-MOF and is in accordance with Laue diffraction studies. Rietveld refinement (Rietveld, 1969) of the patterns was carried out using the GSAS software (Larson and Von Dreele, 2000) along with the graphic user interface software EXPGUI (Toby, 2001). Refined pattern along with experimental data is shown in Figure 5. The Rietveld refined lattice parameters of the MOFs are given in Table III. The lattice parameters of Mn-MOF, $a = 8.3281(03)$ Å, $c = 22.8874(16)$ Å, and $V = 1374.72(01)$ Å^3, compare well with the earlier report on single crystal (Mączka, 2014). The model data are taken from the single-crystal diffraction result, whereas here the crystal is subjected to some pressure while crushing for powder XRD measurement. The differences in intensities observed and calculated may be because of various factors such as the stacking fault introduced while crushing the crystals and poor scattering factors for C, H, and N atoms present in the MOFs.

The lattice parameters and unit-cell volume are found to decrease with substituent in the order Zn, Ni, Co (shown in Figure 6). The reason for such a variation can be understood based on the Shannon ionic radii (Shannon, 1976). The ionic radius (IR), even for a given valance state, depends also on the occupation of orbital by the unpaired electron, i.e. the spin configuration of the ions. There are two spin states, high and low for Mn^{2+} and Co^{2+}, whereas Zn^{2+} and Ni^{2+} have single spin configuration. Zn^{2+} being d^{10} ion diamagnetic, it carries no net magnetic moment and has no

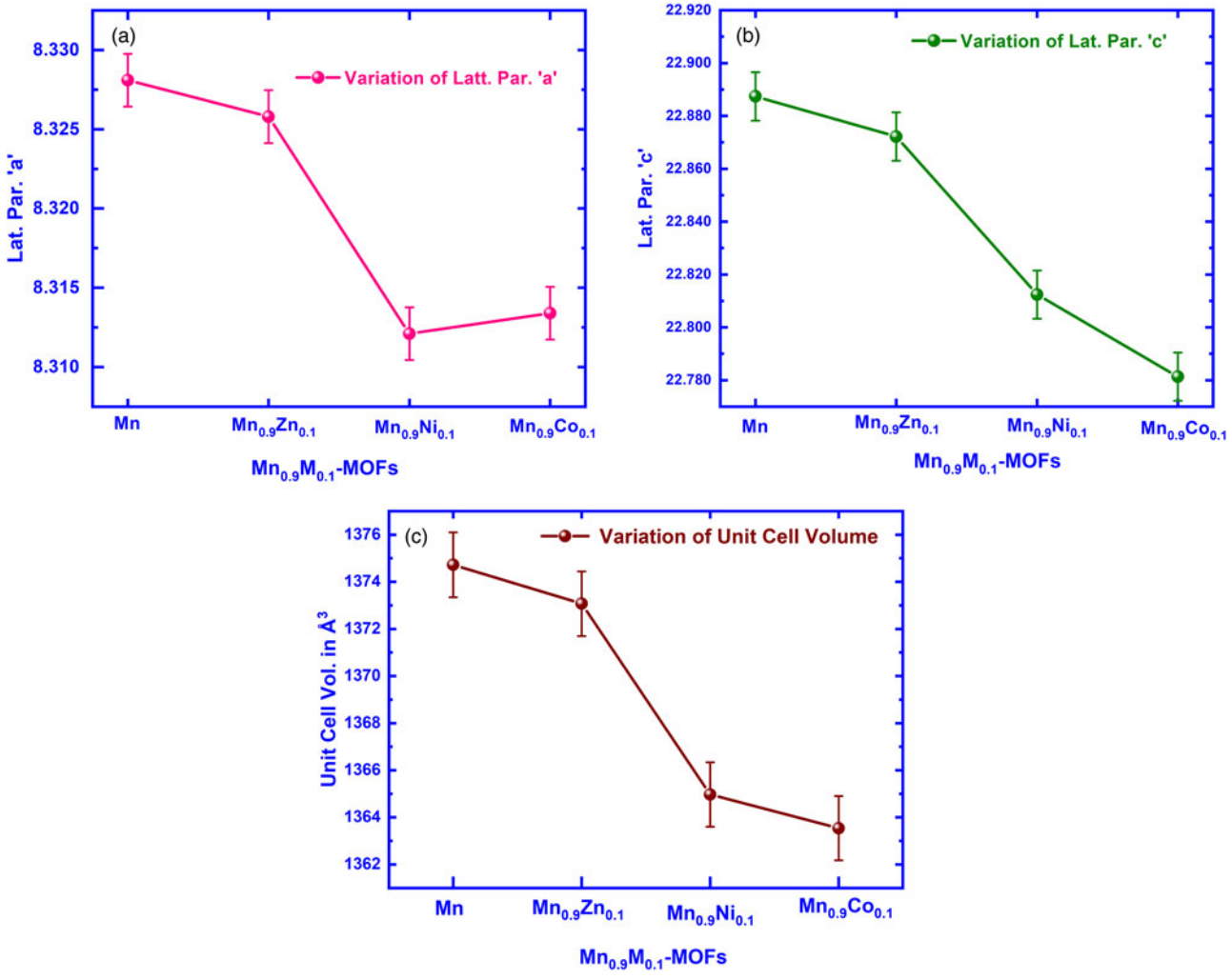

Figure 6. Variation of lattice parameter unit-cell parameters with a substituent for the MOFs: (a) a, (b) c, and (c) unit-cell volume.

https://doi.org/10.1017/S0885715619000307 Published online by Cambridge University Press

TABLE IV. High-spin and low-spin Shannon ionic radii of Mn, Zn, Co, and Ni elements.

Ion	Charge state	Co-ordination	Spin state	Ionic radius Å
Mn	2+	VI	High spin	0.83
			Low spin	0.67
Zn	2+	VI	–	0.74
Ni	2+	VI	–	0.69
Co	2+	VI	High spin	0.745
			Low spin	0.65

spin state. The IR of these four elements is given in Table IV. Shannon IR of Zn^{2+} is smaller than that of Mn^{2+}. Hence both the lattice parameters *a* and *c* decrease. This implies anisotropic bonding of Zn^{2+} with surrounding ligand anions O^{2-}. Both the lattice parameters of Co and Ni substituted MOF are smaller than that of Mn-MOF. This is in accordance with their smaller IR compared with that of Mn^{2+}.

Using the lattice parameters obtained from the Rietveld refinement, the observed peak positions (in $2\theta^{\circ}$) were given as input to the NBS*AIDS83 program which is the up-graded version of NBS*Aids80 (Mighell, *et. al,*1981), without the Miller indices, and the output of this program was used to generate the standard ICDD database files. The Rietveld refined values as well as the NBS*AIDS83 results of these materials all agree with each other and are given in Table III.

IV. CONCLUSION

Single crystals of Mn-, $Mn_{0.9}Zn_{0.1}$-, $Mn_{0.9}Ni_{0.1}$-, and $Mn_{0.9}Co_{0.1}$-MOFs were grown successfully by solvothermal reaction followed by slow evaporation. The single-crystalline nature was confirmed by Laue diffraction method. The lattice parameters were obtained by Rietveld refinement as well as NBS*Aids83 refinements of the powder diffraction patterns. The Mn- and $Mn_{0.9}Zn_{0.1}$-MOFs have meager variations in the unit-cell volume as well as lattice parameters, similarly $Mn_{0.9}Co_{0.1}$- and $Mn_{0.9}Ni_{0.1}$-MOFs are with little difference but have considerable variation in the lattice parameters with respect to Mn- and $Mn_{0.9}Zn_{0.1}$-MOFs. This variation of unit-cell volume is understood based on the Shannon IR.

SUPPLEMENTARY MATERIAL

The supplementary material for this article can be found at https://doi.org/10.1017/S0885715619000307

ACKNOWLEDGEMENT

The author (D.S.) acknowledges P.K. Ajikumar and UGC-DAE CSR, Kalpakkam node for the SEM and EDAX measurements. The authors also acknowledge the constant support and encouragement from IGCAR management.

SUPPLEMENTAL DATA

The NBS*AIDS83 outputs in ICDD file format are given in Tables 5–8 and are attached in the electronic Supplementary material. The images of the experimental and simulated XRD patterns based on the Rietveld refined parameters of all the four MOFs are given in the Supplementary material. The crystallographic information (CIF) files are attached separately.

Baker, P. J., Lancaster, T., Franke, I., Hayes, W., Blundell, S. J., Pratt, F. L., Jain, P., Wang, Z. M., and Kurmoo, M. (**2010**). "Muon spin relaxation investigation of magnetic ordering in the hybrid organic-inorganic Perovskites $[(CH_3)_2NH_2]M(HCOO)_3$ (M=Ni,Co,Mn,Cu)," Phys. Rev. B **82**, 012407.

Jain, P., Ramachandran, V., Clark, R. J., Zhou, H. D., Toby, B. H., Dalal, N. S., Kroto, H. W., and Cheetham, A. K. (**2009**). "Multiferroic behavior associated with an order-disorder hydrogen bonding transition in metal-organic frameworks (MOFs) with the Perovskite ABX_3 architecture," J. Am. Chem. Soc. **131**, 13625–13627.

Larson, A. C. and Von Dreele, R. B. (**2000**). "General Structure Analysis System (GSAS)," Los Alamos National Laboratory Technical Report LAUR 86-748, 2004.

Mączka, M., Gągor, A., Macalik, B., Pikul, A., Ptak, M., and Hanuza, J. (**2014**). "Order-disorder transition and weak ferromagnetism in the Perovskite metal formate frameworks of $[(CH_3)_2NH_2][M(HCOO)_3]$ and $[(CH_3)_2ND_2][M(HCOO)_3]$ (M=Ni, Mn)," Inorg. Chem. **53**, 457–467.

Mighell, A. D., Hubbard, C. R., and Stalick., J. K. (**1981**). NBS*AIDS80, A FORTRAN program for crystallographic data evaluation. *NBS* (*U.S.*) *Technical Note* 1141. Gaithersburg, MD; U.S. Department of Commerce, (NBS*Aids83 is upgraded from NBS*Aids80).

Rietveld, H. M. (**1969**). "A profile refinement method for nuclear and magnetic structure," J. Appl. Crystallogr. **2**, 65–71.

Sánchez-Andújar, M., Presedo, S., Yáñez-Vilar, S., Castro-García, S., Shamir, J., and Señarís-Rodríguez, M. A. (**2010**). "Characterization of the order-disorder dielectric transition in the hybrid organic-inorganic Perovskite-like formate Mn(HCOO)3[(CH3)2NH2]," Inorg. Chem. **49**, 1510–1516.

Schneider, C. A., Rasband, W. S., and Eliceiri, K. W. (**2012**). "NIH image to ImageJ: 25 years of image analysis," Nat. Methods **9**, 671–675.

Shannon, R. D. (**1976**). "Revised effective ionic radii and systematic studies of inter atomic distances in halides and chaleogenides," Acta Crystallogr. **A32**, 751–767.

Thomson, R. I., Jain, P., Cheetham, A. K., and Carpenter, M. A. (**2012**). "Elastic relaxation behavior, magnetoelastic coupling, and order-disorder processes in multiferroic metal-organic frameworks," Phys. Rev. B **86**, 214304.

Toby, B. H. (**2001**). "EXPGUI, a graphical user interface for GSAS," J. Appl. Crystallogr. **34**, 210–213.

Wang, W., Yan, L.-Q., Cong, J.-Z., Zhao, Y.-L., Wang, F., Shen, S.-P., Zou, T., Zhang, D., Wang, S.-G., Han, X.-F., and Sun, Y. (**2013**). "Magnetoelectric coupling in the paramagnetic state of a metal-organic framework," Sci. Rep. **3**, 2024.

Zhao, H., Huang, Z., Ma, Z., Jia, T., Kimura, H., Fu, Q., Wang, G., Tao, H., Cai, K., and Fa, Z. (**2017**). "Structural, magnetic and dielectric properties of $[(CH_3)_2NH_2]Fe_xMn_{1-x}(HCOO)_3$," J. Electron. Mater. **46**, 5540–5545.